Supporting Information:

X-ray Absorption Spectroscopic Investigation of the Electronic Structure Differences in Solution and Crystalline Oxyhemoglobin

Samuel A. Wilson,[a,c] Evan Green,[b,c] Irimpan Mathews,[c] Maurizio Benfatto,[d] Keith O. Hodgson,[a,c] Britt Hedman,[c] and Ritimukta Sarangi[c,*]

[a]*Department of Chemistry, Stanford University, CA 94305*

[b]*Department of Chemistry, Reed College, Portland, OR 97202*

[c]*Stanford Synchrotron Radiation Lightsource, SLAC National Accelerator Laboratory, Menlo Park, CA 94025*

[d]*Laboratori Nazionali di Frascati dell' INFN, C.P. 13, 00044, Frascati, Italy*

Table of Contents

Experimental Methods:

Sample Preparations

All reagents were obtained from Sigma-Aldrich Co. as the highest purity available and were used without further purification. All anaerobic solutions were prepared by degassing solvents in a Schlenk link by five freeze-pump-thaw cycles under an argon atmosphere.

Hemoglobin Proteins

Deoxy-hemoglobin (hemoglobin = Hb) was prepared based on the work of Di Iorio *et al.* (1). Under an inert atmosphere, 1.29 g (2.0 mmol) of lyophilized aquamet bovine (2) Hb was dissolved in 10 mL of pH ~7.5 buffer solution (0.1 M NaH_2PO_4 and 0.5 mMol Na_2EDTA). Part of this sample was saved as aquamet-Hb and part of the samples was treated with a 10-fold excess of sodium dithionite (69.6 mg) reducing the iron from Fe^{3+} to Fe^{2+}. The protein was then filtered using a Sephadex G-25 column to remove any extraneous iron and denatured protein. The solution was then concentrated by centrifugation to ~8 mM in iron. Oxy-Hb was prepared by exposing the above deoxy-Hb to a pure O_2 atmosphere for a period of 10-15 minutes. Oxygenation was continuously monitored by UV-vis until the spectrum stabilized. Hydroxymet-Hb was prepared by slowly raising the pH of aquamet-Hb to 11 (monitored using a pH meter) by drop wise addition of a concentrated NaOH solution. X-ray absorption spectroscopy (XAS) samples were loaded into 2 x 10 mm pinhole cells and frozen with a pentane slush.

Iron TPP Model Complexes

All model synthesis was performed inside an O_2 and moisture free glove box to avoid air oxidation of the ferrous systems. $[Fe^{II}(TPP)]$ (TPP = *meso*-tetraphenylporphyrin) was prepared by the reduction of 10 mM $[Fe^{III}(TPP)Cl]$ using Zn/Hg in toluene solution. A heterogeneous mixture of 5 mM $[Fe^{III}(TPP)Cl]$ was stirred with Zn/Hg for 2 hours and the final reduced product was collected via filtration. The reduction was followed by UV-vis spectroscopy ensuring a complete reduction from Fe^{3+} to Fe^{2+}. $[Fe^{II}(TPP)(py)_2]$, $[Fe^{II}(TPP)(ImH)_2]$ and $[Fe^{II}(TPP)(THF)_2]$ were prepared by the addition of a ~5 fold excess of pyridine, imidazole, or tetrahydrofuran, respectively to the $[Fe^{II}(TPP)]$ solution. $[Fe^{III}(TPP)(ImH)_2]Cl$ was synthesized according to published methods (3). 500 mg (0.71 mmol) of $[Fe^{III}(TPP)Cl]$ was mixed with six equivalents of ImH in 60 mL of $CHCl_3$. Crystals of which were obtained directly by hexane diffusion. The final concentration of all model complexes in solution was between 4–5 mM in Fe. The samples were loaded into XAS cells equipped with 37 μm Kapton windows inside the glove box, immediately frozen, and stored under liquid N_2. During data collection, the samples were maintained at a constant temperature of ~10 K using an Oxford Instruments CF 1208 liquid helium cryostat.

Fe K-edge XAS: Solution Measurements

Fe K-edge XAS data on the solution samples were measured on the unfocussed 20 pole 2 T wiggler side-station beamline 7-3, which is the standard biological solution XAS beamline at Stanford Synchrotron Radiation Lightsource (SSRL). The data were collected under standard ring conditions of 3 GeV and ~100 mA ring current. A Si(220) double-crystal monochromator was used for energy selection while a Rh-coated mirror was used for harmonic rejection. Spectra were collected in the fully tuned configuration of the monochromator. Data on the solution samples were measured in fluorescence mode using a Canberra 100-element solid-state Ge monolith detector. Internal energy calibration was accomplished by simultaneous measurement of the absorption of a Fe foil placed between two ionization chambers situated after the sample. The first inflection point of the foil spectrum was fixed at 7111.2 eV. The solution samples were monitored for photoreduction throughout the course of data collection. The oxy-Hb (small shift), aquamet-Hb and hydroxymet-Hb showed edge-shifts associated with photoreduction and thus a single scan was collected on each spot for these samples across multiple XAS cells. The spectra presented here are 5–10 scan averages, which were sufficient to obtain a good signal to noise ratio in the near-edge region. 20 scans were collected on the oxy-Hb sample in order to obtain good signal to noise in the

extended X-ray absorption fine structure (EXAFS) region. A similar data reduction protocol was followed for all data sets. A third-order polynomial was fit to the pre-edge region and subtracted from the entire spectrum as background ensuring a flat pre-edge and post-edge region. A three-region spline of orders 2, 3, and 3 used to model the smoothly decaying post-edge region. The data were normalized using the Pyspline (4) program by subtracting a cubic spline and assigning the edge jump to 1.0 at 7200 eV.

Theoretical EXAFS signals, $\chi(k)$, were calculated using *FEFF* (Macintosh version 8.4) (5-7) and the X-ray crystal structure of oxy-Hb (2DNI) (8), with theoretical models fit to the data using EXAFSPAK (9). The structural parameters varied during the fitting process were the bond distances (R) and the bond variance σ^2, which is related to the Debye-Waller factor resulting from thermal motion and static disorder of the absorbing and scattering atoms. The non-structural parameter E_0 (the energy at which the photoelectron wave vector k is zero) was also allowed to vary but was restricted to a common value for every component in a given fit. Coordination numbers were systematically varied in the course of the fit but fixed within a given fit.

The areas under the Fe K pre-edge region were quantitated using the Edg_Fit program (9), which is part of the EXAFSPAK suite of programs. Psuedo-Voigt functions with 1:1 Gaussian:Lorentzian mixing were used to fit the pre-edge by a similar protocol to that previously published (10). The error in pre-edge intensities and energy positions were calculated by comparing several good fits over different energy ranges. The typical error in intensity estimation was ~5% and the error in energy position was < 0.1 eV.

Fe K-edge XAS: Single Crystal Measurements

Single crystal Fe K-edge XAS measurements were performed on oxy-Hb crystals (~300 um in size) on the 16 pole, 2 T wiggler beamline 9-3 at SSRL under standard ring conditions of 3 GeV and ~100 mA ring current. A Si(220) double-crystal monochromator was used for energy selection. Other optical components used for the experiments were a Rh-coated harmonic rejection mirror and a cylindrical Rh-coated bent focusing mirror. Spectra were collected in the fully tuned configuration of the monochromator. Fe K near-edge data were collected in the fluorescence mode using a Canberra 30-element solid-state Ge detector. Multiple crystals were used on the same loop to obtain isotropic data. Because of this, and since the unit cell has 4 dissimilarly oriented heme groups, no polarization effects were observed in the data. An Oxford Instruments open flow liquid He cryostat was used to maintain the sample temperature at ~30 K throughout the course of the measurement. The crystalline samples did not show discernible amounts of photoreduction between scans, and therefore five scans were averaged to obtain a good signal to noise ratio in the data.

UV-vis Measurements

UV-visible spectra on the different forms of hemoglobin were measured over the range 190–820 nm using a Hewlett-Packard 8452A diode array spectrophotometer. Fresh blank scans were recorded before each measurement. Reaction solutions were sealed in anaerobic Spectrosil quartz cuvettes of 10 mm path length using silicone-greased 14/35 ground glass caps. These cuvettes are capable of maintaining N,N-dimethylformamide solutions of iron(II)-tetraethanethiolate ($E_{1/2}$ = ~ –1V vs. NHE) overnight in air without detectable oxidation (11).

DFT Calculations

Gradient corrected, (GGA) spin unrestricted density functional theory (DFT) calculations were performed using ORCA 2.8 (12, 13) on a 12-cpu Linux cluster. The BP86 (14-16) local functional and the following basis sets were employed for the calculations: the core properties, triple-ζ basis set CP(PPP) (17) with three polarization functions on Fe, the Ahlrich's all electron TZVP (18, 19) on all other atoms. Tight convergence criteria were imposed on all calculations. Calculations were performed in a dielectric continuum using the conductor like screening model (COSMO) (20) with CH_2Cl_2 as the dielectric medium for all model complexes and a dielectric constant of 10 for all

protein systems. For the protein systems, starting guess geometries were obtained from crystal structures. For oxy-Hb the crystal structure from 2DNI was used due to its high resolution (1.25 Å), and all heme groups were truncated to octa-methyl porphyrins. The *trans*-axial histidine was modified to include the Cα of the amino acid, and was fixed for all calculations. The distal histidine H-bonding to the O_2 group was similarly modified and the Cα fixed. A water molecule was used instead of the O(glu) ligand to mimic the H-bonding interaction to the *trans*-axial histidine the N1(His)–O(glu) distance was fixed at 2.8 Å. For the constrained crystal calculation the ConstrainFragment keyword in ORCA was employed. The protein based ligands (see schematic below) and the heme group structure was fixed. The Fe, the O_2, and all the H-atoms in the structure were allowed to optimize.

Time-dependent (TD)-DFT calculations were performed with the electronic structure program ORCA to calculate the energies and intensities of the Fe K pre-edges (21). The tight convergence criterion was imposed on all calculations. The calculated energies and intensities were Gaussian broadened with half-widths of 1.5 eV to account for core-hole lifetime and instrument resolution. The calculated pre-edge energy positions were shifted up by ~182.5 eV to match the experimental spectra. This is generally the case with core level TD-DFT calculations since DFT does not describe core potentials accurately, resulting in the core levels being too high in energy relative to the valence levels.

MXAN Near-edge Analysis

The geometric structures of solution and crystalline oxyHb were extracted from the XANES data using the MXAN program (Minuit XANes). The scattering path operator was calculated exactly without any series expansion to include the XANES region in the calculation and fit; avoiding any *a-priori* selection of the relevant multiple-scattering (MS) paths. The Muffin-Tin (MT) approximation was used for the shape of the potential and hydrogen atoms were not included in the calculation. Details of the program have been reported elsewhere (22). The function minimized during the MXAN fit was R_{sq}, defined as:

$$R_{sq} = n \frac{\sum_{i=1}^{m} w_i [(y_i^{th} - y_i^{\exp}) \varepsilon_i^{-1}]^2}{\sum_{i=1}^{m} w_i}$$

where, "n" is the number of independent parameters, "m" is the number of data points, "y_i^{th}" and "y_i^{exp}" are the theoretical and experimental values of the absorption, respectively, "ε_i" is the error in each point of the experimental data set, and "w_i" is a statistical weight. When $w_i = 1$, the square residual function R_{sq} becomes the statistical χ^2 function. In this work, $w_i = 1$ was assumed and the experimental error ε = constant = 1.0% of the main experimental edge jump over the whole data set. Statistical errors were calculated using the MIGRAD routine. MXAN also introduces a systematic error of 1–2% into the bond lengths that must be added to the MIGRAD statistical error.

MXAN has been successfully used in the past to fit Fe K-edge XANES data in hemoglobin and myoglobin (23-25). The fits presented herein, were performed by first excluding and then including the O_2 and refining the first shell distances. Inclusion of the O_2 group resulted in a significant lowering in the R_{sq} value for both solution and crystalline oxy-Hb. During the course of the optimization, the porphyrin ring distances were linked to the ligating pyrollic N atoms. The starting active site structure was the modified from the crystal structure 2DNI. Complete refinement of the non-structural parameters including the Muffin-Tin radii was performed. The error in the first shell bond distances is ~0.05 Å.

Supporting Tables:

SI Table S1. EXAFS Least Squares Fitting Results for Oxy-Hemoglobin.

Coordination / Path	R (Å)[a]	σ^2 (Å^2)[b]	E_0 (eV)	F[c]
1 Fe–O	1.83	462		
5 Fe–N	2.02	222		
8 Fe–C	3.04	353		
16 Fe–C–N[d]	3.17	353	–4.14	0.37
4 Fe–C	3.39	255		
8 Fe–N	4.08	531		
16 Fe–C–N[d]	4.34	531		

[a]The estimated standard deviations for the distances are in the order of ± 0.02 Å. [b]The σ^2 values are multiplied by 10^5. [c]Error (*F*) is given by $\Sigma[(\chi_{obsd} - \chi_{calcd})^2 k^6]/\Sigma[(\chi_{obsd})^2 k^6]$. [d]The σ^2 value for the Fe–C (single scattering) and Fe–C–N (multiple scattering) paths were fixed to be the same value.

SI Table S2. TD-DFT Calculated Average Energies and Intensities.

	Energy (eV)	Calculated Area[a]
$[Fe^{II}(TPP)(Py)_2]$ (Pauling Model)	7112.7	2.21
Oxy-Hemoglobin	7112.7	1.55
Hydroxymet-Hemoglobin (Weiss Model)	7112.1	0.93

[a]The calculated areas are based on dipole (D^2) and electric and magnetic quadrupole (Q^2 and M^2) contributions respectively.

SI Table S3. XAS Pre-edge Energy and Intensity.

	Peak 1 (eV)	Area	Peak 2 (eV)	Area	Peak 3 (eV)	Area	Total Intensity
$[Fe^{III}(TPP)(ImH)_2]Cl$	7111.1	0.8	7112.8	4.7	7114.1[a]	1.1[a]	5.5 ± 0.2
$[Fe^{II}(TPP)(ImH)_2]$	7112.2	4.7	7114.8[a]	1.1[a]			4.7 ± 0.4
Oxy-Hb Solution[b]	7111.3	0.8	7112.7	7.8	7114.5[a]	2.0[a]	8.6 ± 0.5
Oxy-Hb Solution[c]	7112.7	8.4	7114.4[a]	1.7[a]			8.4 ± 0.6
Oxy-Hb Crystal[d]	7112.3	5.6	7114.7[a]	0.8[a]			5.6 ± 0.4

Fe K pre-edge fits for low-spin ferric $[Fe^{III}(TPP)(ImH)_2]Cl$ and ferrous $[Fe^{II}(TPP)(ImH)_2]$ compared to solution and crystallized oxy-hemoglobin. Peak energies are listed at maximum, areas are multiplied by 100 for convenience and comparison to previously published data. [a]Total intensity is the sum of the areas but does not include the highest energy feature of any fit. [b]Oxy-hemoglobin solution pre-edge fit as low-spin ferric with two features. [c]Oxy-hemoglobin solution pre-edge fit as low-spin ferrous with one feature. [d]Oxy-hemoglobin crystal fit as low-spin ferrous with one feature. Error values are calculated from total intensity standard deviations across all nine fits. Fits are shown in SI Figure 4 and 8.

SI Table S4. DFT Calculated Bond Distances.

Oxy-Hb Models	Model	Fe–O	O–O	Fe–N(His)	Fe–N Equatorial[b]
2 H-Bonds, ε =10	1	1.826	1.323	2.051	2.01
H-Bond Only to O_2, ε = 10	2	1.760	1.317	2.072	2.01
H-Bond Only to Axial His, ε = 10	3	1.832	1.306	2.072	2.01
No H-Bonds, ε = 10	4	1.762	1.304	2.089	2.01
2 H-Bonds, ε = 1	5	1.821	1.304	2.074	2.01
H-Bond Only to O_2, ε = 1	6	1.758	1.302	2.093	2.01
H-Bond Only to Axial His, ε = 1	7	1.825	1.290	2.110	2.01
No H-Bonds ε = 1	8	1.762	1.285	2.116	2.01

[a]2 H-bonds indicates the H-bonds to axial His and the O_2. The different dielectric constants (10 and 1) represent protein environment and vacuum. [b]Average equatorial Fe–N(heme) distance. All distances given in Å.

Supporting Schemes:

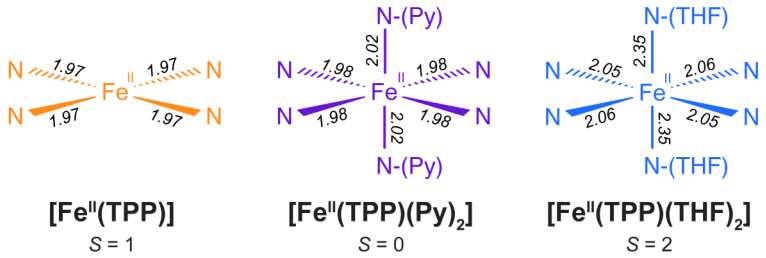

[Fe^{II}(TPP)] *S* = 1 **[Fe^{II}(TPP)(Py)$_2$]** *S* = 0 **[Fe^{II}(TPP)(THF)$_2$]** *S* = 2

SI Scheme S1. The first shell bond distances in the Fe^{2+} (S = 0, 1, 2) model complexes [Fe^{II}(TPP)], [Fe^{II}(TPP)$(Py)_2$] and [Fe^{II}(TPP)$(THF)_2$] respectively.

Supporting Figures:

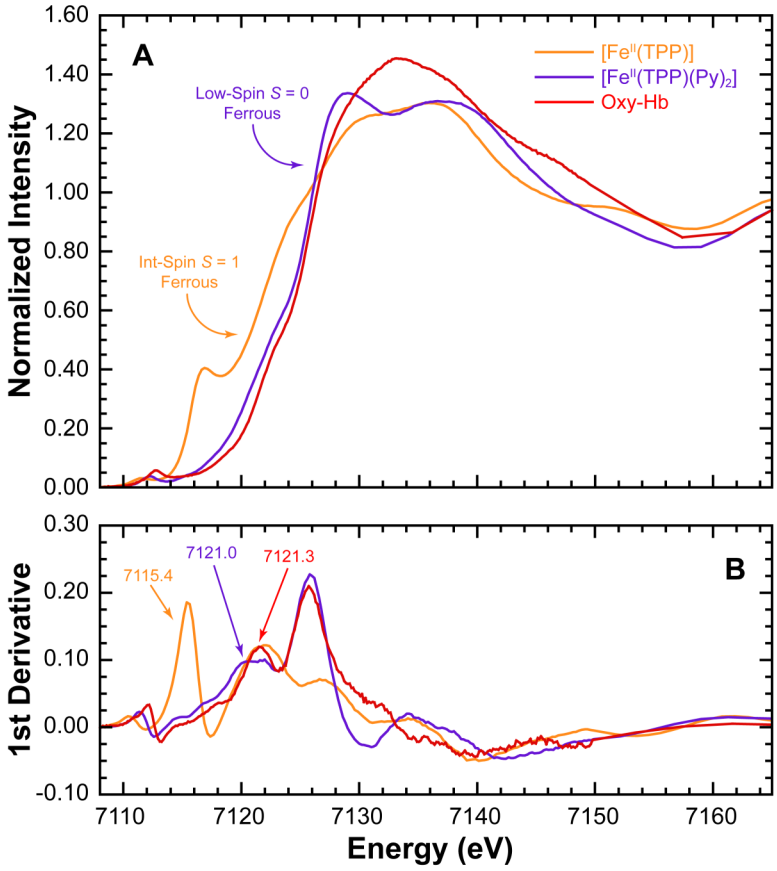

SI Figure S1. (A) Fe K-edge XAS data of intermediate-spin ferrous [Fe^{II}(TPP)] and low-spin ferrous [Fe^{II}(TPP)(Py)$_2$] vs. Oxy-Hemoglobin. (B) The Fe K-edge first derivative spectra with labeled inflection point energies.

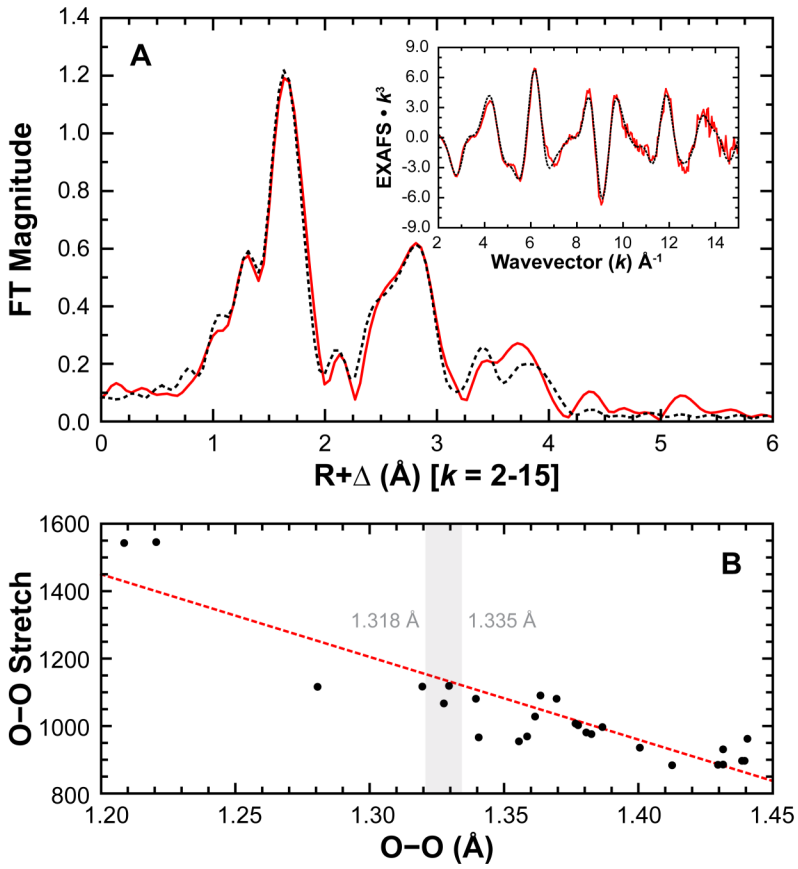

SI Figure S2. (A) Fe non-phase shift corrected FT for EXAFS data and fit (----) for oxy-Hb. Inset shows the corresponding EXAFS region and associated fit. (B) Correlation of crystallographically characterized O–O distances and the O–O stretching frequency obtained from rR data in M–O_2 systems. This correlation has been extended to include mononuclear first-row transition metal M–O_2 systems characterized since the Cramer study (see text). The grey region represents the estimate of O–O distance in oxy-Hb from the O–O rR stretch of oxy-Hb and related species.

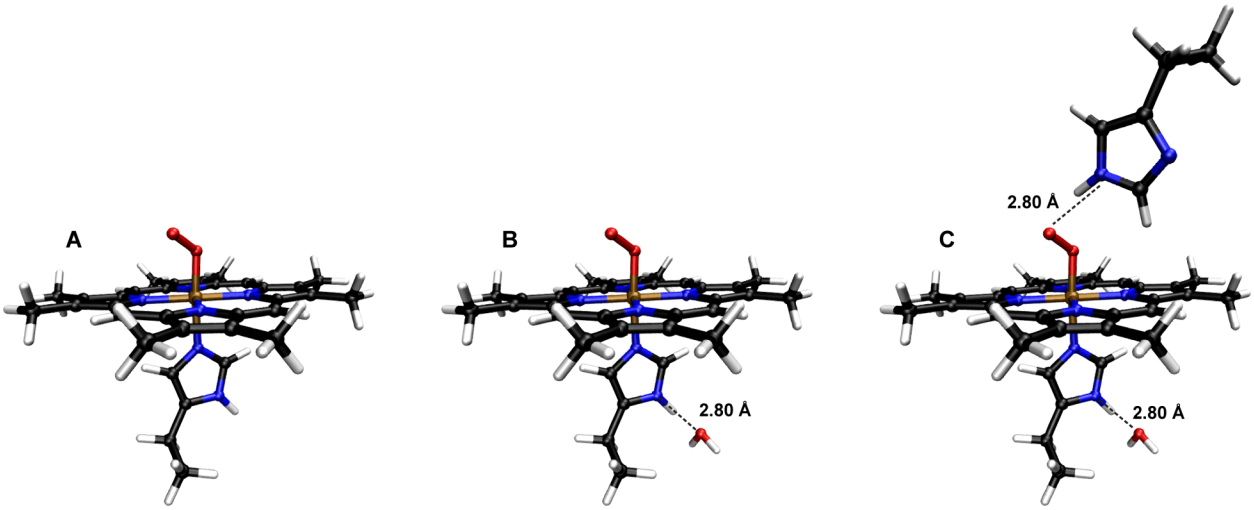

SI Figure S3. Starting structures for the DFT calculations to test the effect of H-bond and dielectric constant. (A) "No H-bonds". (B) "H-bond to axial His". (C) "H-bond to axial His and O_2". The starting structure for the "H-bond to O_2" model is the same as (C) without the water molecule.

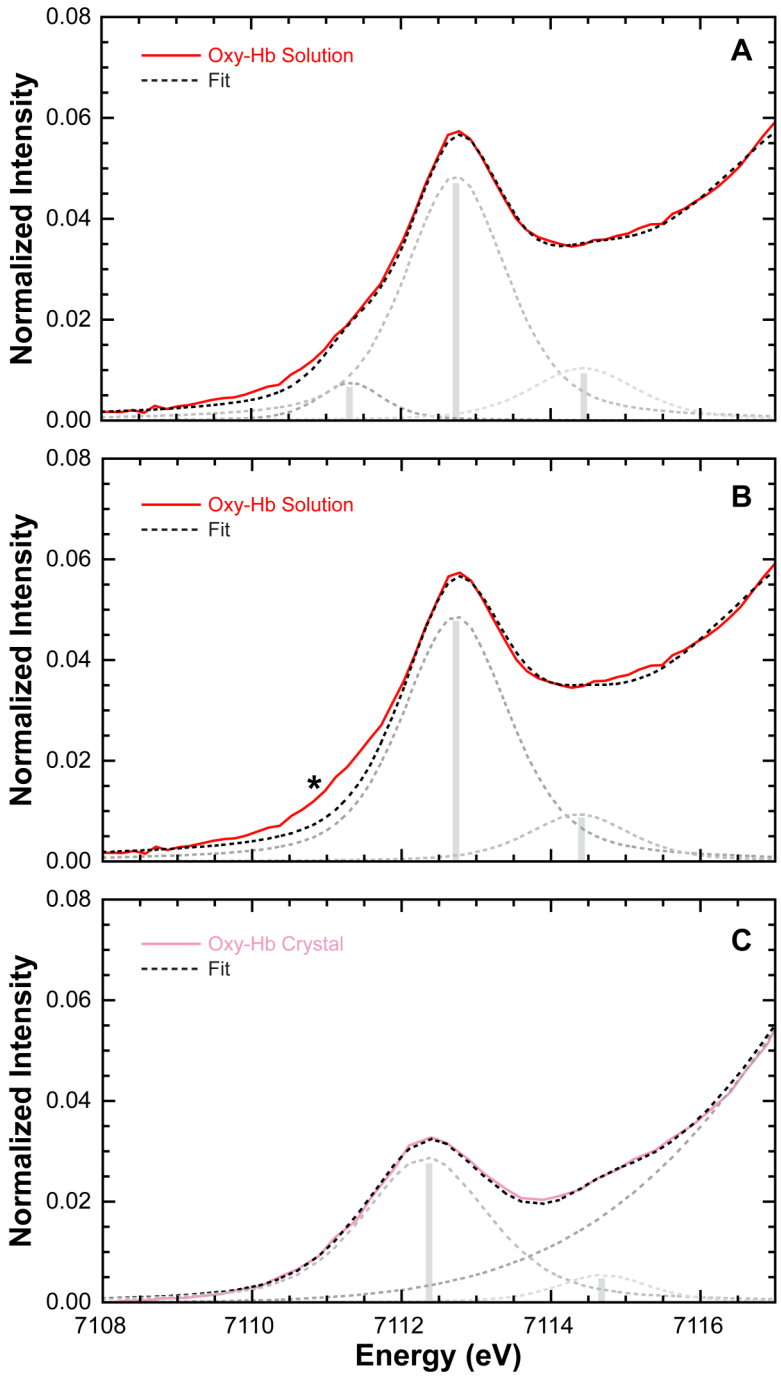

SI Figure S4. Fe K pre-edge XAS data of solution oxy-hemoglobin fit with either three (pane A) or two (pane B) pre-edge features, following the protocol for low-spin ferric or ferrous species $[Fe^{III}(tpp)(ImH)_2]Cl$ and $[Fe^{II}(tpp)(ImH)_2]$, respectively (10). In pane B, the absence of the feature indicated by * underfits the lower energy region of the spectrum. (C) Fe K pre-edge and fit to crystalline oxy-hemoglobin, analogous to low-spin ferrous $[Fe^{II}(tpp)(ImH)_2]$ with a single pre-edge feature. This single features reproduces the pre-edge data and does not underfit the low-energy region of the spectrum as seen in pane B. Reference SI Table S3 for pre-edge fit energy and intensity values.

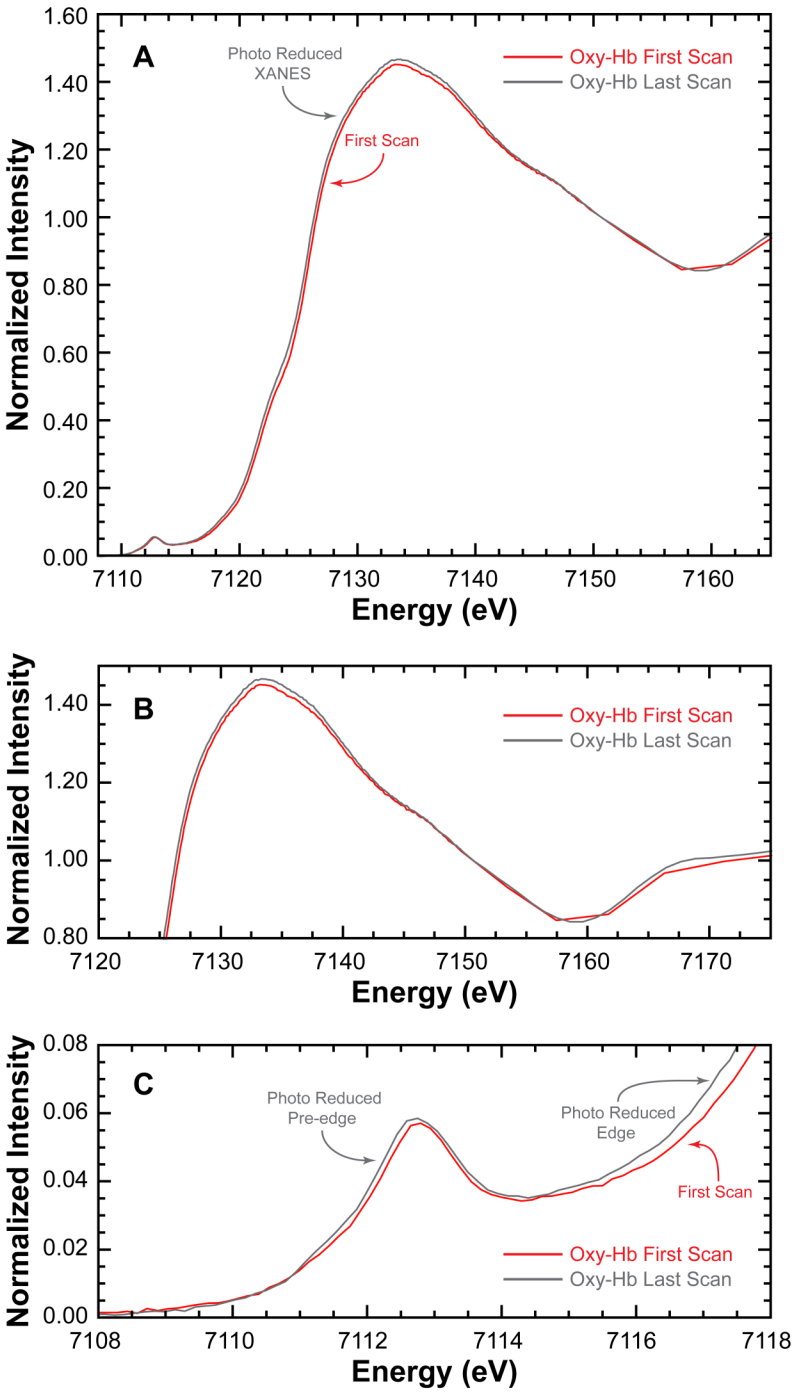

SI Figure S5. Panes A, B, and C show the affects of photoreduction (1st and 4th scan) on the XAS spectrum of oxy-hemoglobin in the K-edge, XANES, and pre-edge regions, respectively. As the figure demonstrates, the shift in the edge is small, but real in the solution data. This shift is significantly less in the crystalline data.

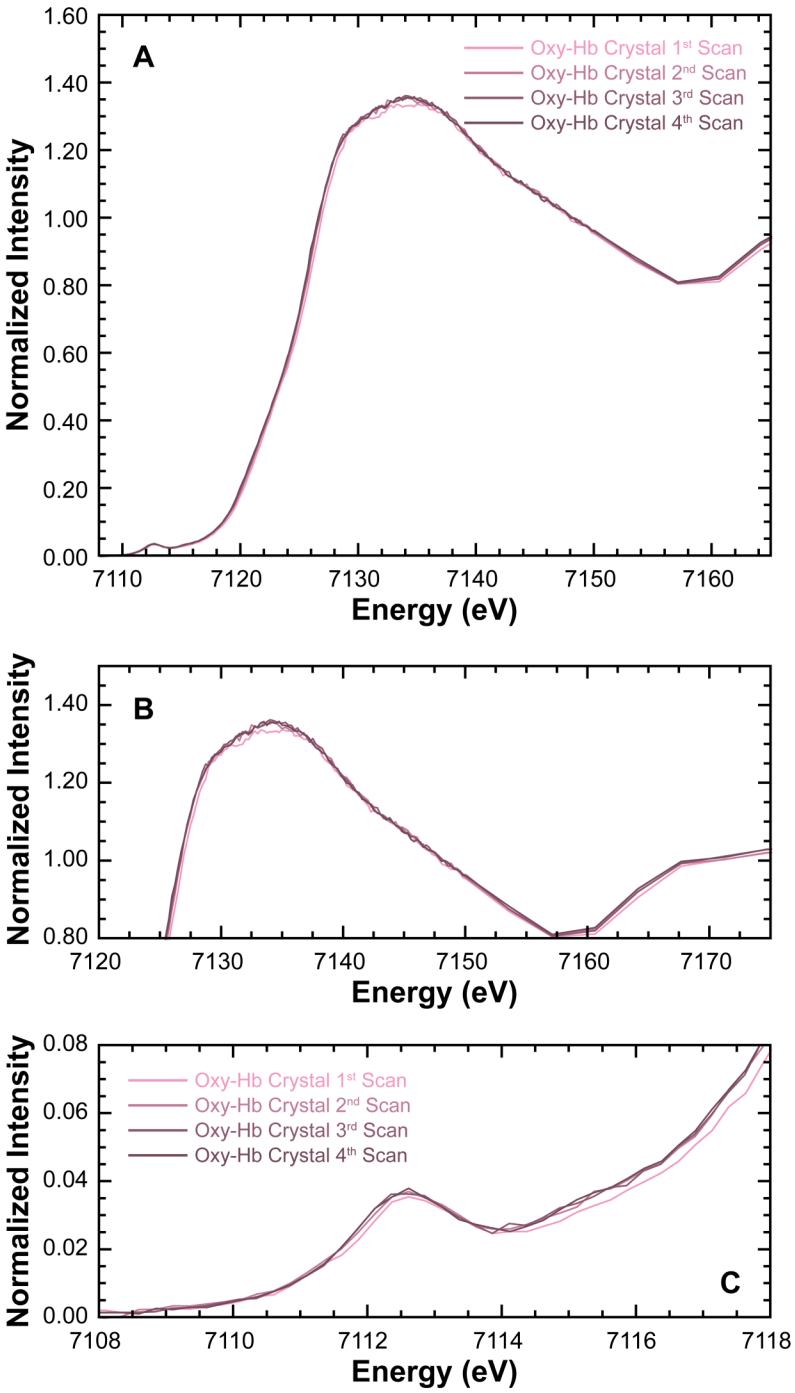

SI Figure S6. Panes A, B, and C show the affects of photoreduction (first through fourth scans) on the XAS spectrum of crystallized oxy-hemoglobin in the K-edge, XANES, and pre-edge regions, respectively.

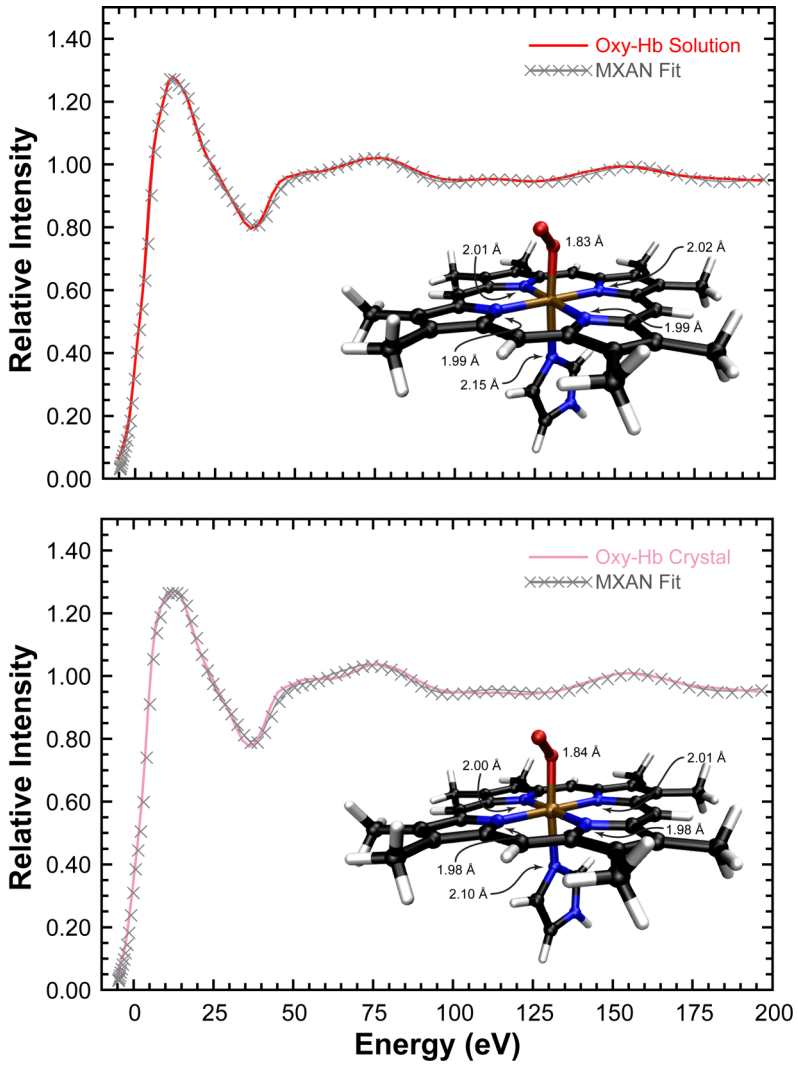

SI Figure S7. X-ray absorption near edge structure (XANES) and MXAN fits to 6-coordinate MXAN models of solution (top) and crystal (bottom) oxy-hemoglobin. Optimized MXAN structures are shown in the inset of each pane with first shell bond lengths, Fe–N and Fe–O, appropriately labeled. Since the error in bond distances is of the order of 0.05 Å, a significant difference cannot be discerned between the two structures. Also note that long-range multiple scattering effects (up to ~ 10 Å) could lead to the small differences observed between the two data sets.

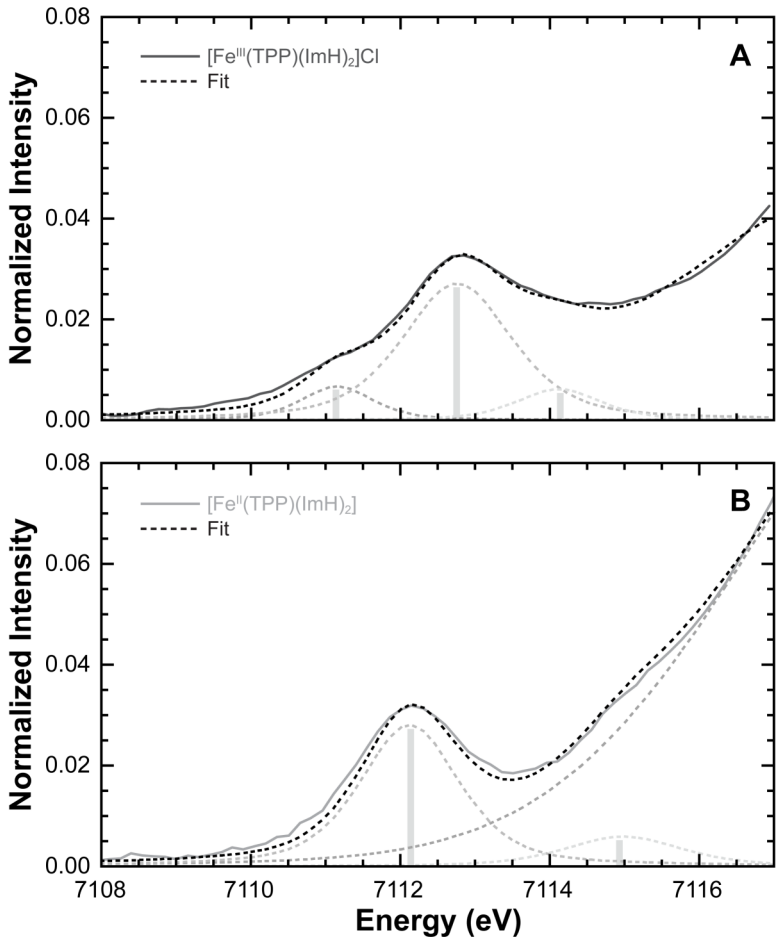

SI Figure S8. Fe K pre-edge XAS data and fits for low-spin ferric $[Fe^{III}(TPP)(ImH)_2]Cl$ and ferrous $[Fe^{II}(tpp)(ImH)_2]$. (A) $[Fe^{III}(TPP)(ImH)_2]Cl$ is well fit with two features with the lower energy representing transitions to states with t_{2g} hole character (10). (B) $[Fe^{II}(tpp)(ImH)_2]$ is well fit with a single feature. Analogous to $[Fe^{III}(tpp)(ImH)_2]Cl$, the high energy feature (~7115 eV) is part of the rising edge and not included in the pre-edge area (SI Table S3).

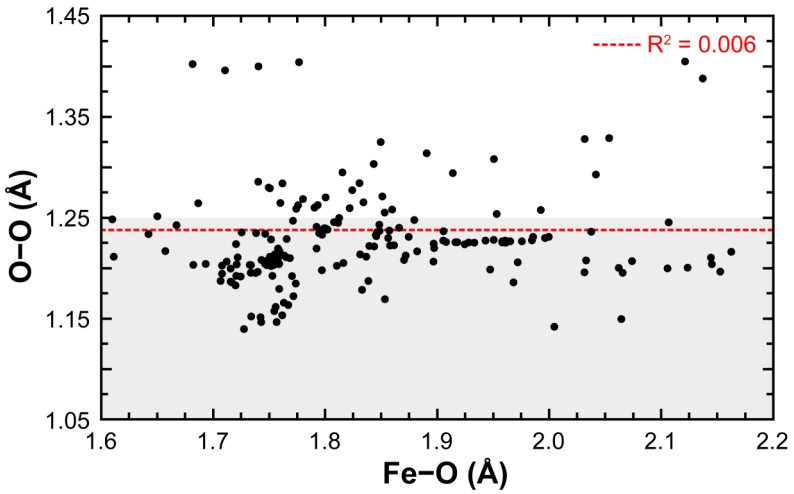

SI Figure S9. A correlation plot between Fe–O and O–O distances obtained from published crystal structures of oxy-Hb, with a resolution better than 2 Å. The red fit line and R^2 value show no correlation between the two distances, however, the majority of O–O distances are shorter than 1.25 Å (shaded region).

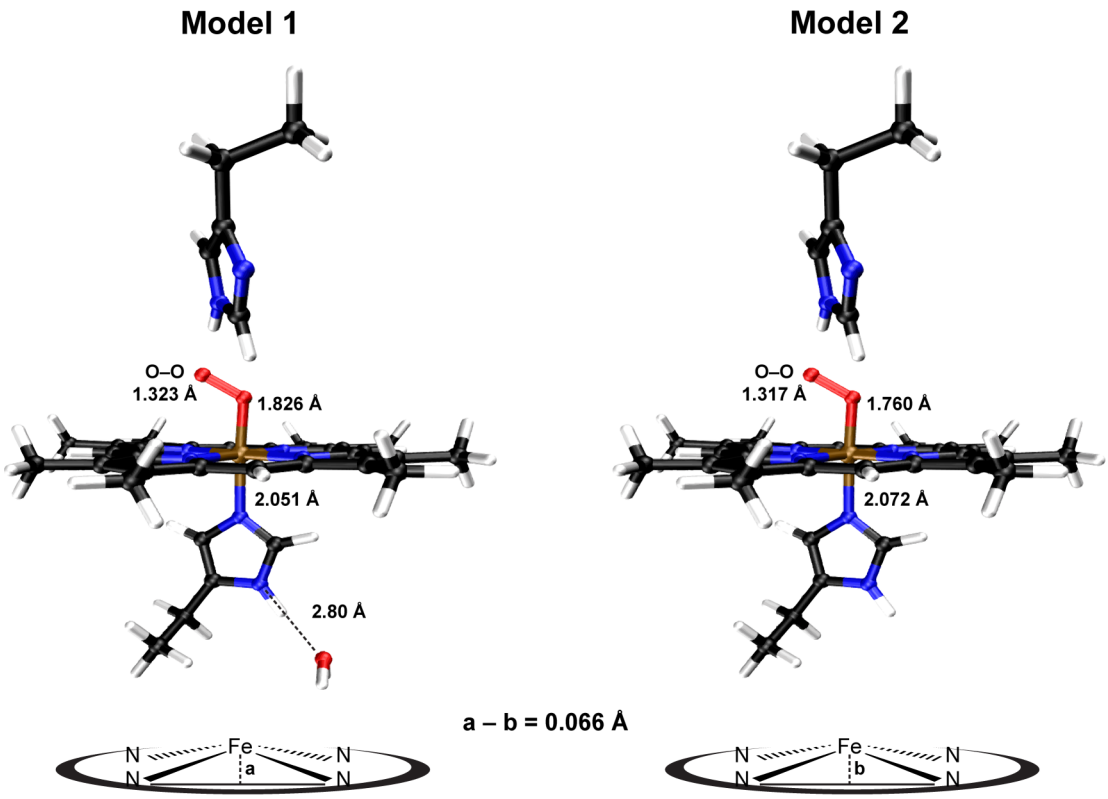

SI Figure S10. DFT optimized structures for Model 1 (with H-bonding to the axial N(His) ligand) and Model 2 (without H-bonding to the axial N(His) ligand). The schematic at the bottom shows the difference in position of the Fe atom in the heme plane. Note that this difference of 0.066 Å is smaller than the 0.116 Å observed in the Collman model complexes (26). It is consistent with the smaller effect on the Fe–O distance in the oxy-Hb models (1.826 – 1.760 = 0.066 Å) compared to the Collman complexes (1.90 – 1.75 = 0.15 Å).

Supporting References:

1. Di Iorio EE (1981) Preparation of Derivatives of Ferrous and Ferric Hemoglobin. *Methods Enzymol.* 76:57-72.
2. Maas BHA, Buursma A, Ernst RAJ, Maas AHJ, & Zijlstra WG (1998) Lyophilized bovine hemoglobin as a possible reference material for the determination of hemoglobin derivatives in human blood. *Clin. Chem.* 44:2331-2339.
3. Scheidt WR, Osvath SR, & Lee YJ (1987) Crystal and molecular structure of bis(imidazole)(meso-tetraphenylporphinato)iron(III) chloride. A classic molecule revisited. *J. Am. Chem. Soc.* 109:1958-1963.
4. Tenderholt A (2007) Pyspline and QMForge. (Stanford University).
5. Mustre de Leon J, Rehr JJ, Zabinsky SI, & Albers RC (1991) Ab initio curved wave x-ray absoprtion fine structure. *Phys. Rev. B 44*(9):4146-4156.
6. Rehr JJ & Ankudinov AL (2003) New developments in the theory and interpretation of X-ray spectra based on fast parallel calculations. *J. Synchrotron Radiat.* 10(Pt 1):43-45.
7. Rehr JJ, Mustre de Leon J, Zabinsky SI, & Albers RC (1991) Theoretical X-ray absorption fine structure standards. *J. Am. Chem. Soc.* 113(14):5135-5140.
8. Park SY, Yokoyama T, Shibayama N, Shiro Y, & Tame JR (2006) 1.25 Å resolution crystal structures of human haemoglobin in the oxy, deoxy and carbonmonoxy forms. *J. Mol. Biol.* 360(3):690-701.
9. George GN (2000) EXAFSPAK and EDG-FIT. (Stanford Synchrotron Radiation Laboratory, Stanford Linear Accelerator Center, Stanford, CA).
10. Westre TE*, et al.* (1997) A multiplet analysis of Fe K-edge 1s→3d pre-edge features of iron complexes. *J. Am. Chem. Soc.* 119(27):6297-6314.
11. Frank P & Hodgson KO (2005) Cooperativity and intermediates in the equilibrium reactions of Fe(II,III) with ethanethiolate in N-methylformamide solution. *J. Biol. Inorg. Chem.* 10(4):373-382.
12. Neese F (2008) ORCA: An Ab initio, DFT and Semiempirical Electronic Structure Package. (Version 2.6.35, University of Bonn, Germany, 2008.).
13. Neese F & Olbrich G (2002) ORCA publication. *Chem. Phys. Lett.* 362:170-178.
14. Becke AD (1988) Density functional exchange-energy approximation with correct asymptotic behaviour. *Phys. Rev. A* 38(6):3098-3100.
15. Becke AD (1993) Density functional theromochemistry:3 the role of exact exchange. *J. Chem. Phys.* 98(7):5648-5652.
16. Perdew JP (1986) Density-functional approximation for the correlation energy of the inhomogeneous electron gas. *Phys. Rev. B* 33:8822-8824.
17. Sinnecker S, Slep LD, Bill E, & Neese F (2005) Reference for CP(PPP). *Inorg. Chem.* 44:2245-2254.
18. Schaefer A, Horn H, & Ahlrichs R (1992) Fully optimized contracted Gaussian basis sets for atoms Li to Kr. *J. Chem. Phys.* 97(4):2571-2577.
19. Schaefer A, Huber C, & Ahlrichs R (1994) Fully optimized contracted Gaussian basis sets of triple zeta valence quality for atoms Li to Kr. *J. Chem. Phys.* 100(8):5829-5835.
20. Sinnecker S, Rajendran A, Klamt A, Diedenhofen M, & Neese F (2006) Calculation of solvent shifts on electronic g-tensors with the conductor-like screening model (COSMO) and its self-consistent generalization to real solvents (direct COSMO-RS). *J. Phys. Chem. A* 110(6):2235-2245.
21. Chandrasekaran P*, et al.* (2011) Prediction of high-valent iron K-edge absorption spectra by time-dependent density functional theory. *Dalton Trans.* 40(42):11070-11079.
22. Sarangi R*, et al.* (2012) The x-ray absorption spectroscopy model of solvation about sulfur in aqueous L-cysteine. *J. Chem. Phys.* 137(20):205103.
23. Arcovito A*, et al.* (2005) Light-induced relaxation of photolyzed carbonmonoxy myoglobin: a temperature-dependent x-ray absorption near-edge structure (XANES) study. *Biophys. J.* 88(4):2954-2964.

24. Della Longa S, *et al.* (2003) Redox-induced structural dynamics of Fe-heme ligand in myoglobin by X-ray absorption spectroscopy. *Biophys. J.* 85(1):549-558.
25. Della Longa S, *et al.* (2001) Structure of the Fe-heme in the hemodimeric hemoglobin from Scapharca inaequivalvis and in the T721 mutant: an X-ray absorption spectroscopic study at low temperature. *Eur. Biophys. J.* 29(8):559-568.
26. Jameson GB, *et al.* (1980) Models for the active site of oxygen-binding hemoproteins. Dioxygen binding properties and the structures of (2-Methylimidazole)-meso-tetra(α,α,α,α-o-pivalamidophenyl) porphyrinatoiron(II)-ethanol and Its dioxygen adduct. *J. Am. Chem. Soc.* 102:3224-3237.